Available online at www.sciencedirect.com

ScienceDirect

Ceramics International 42 (2016) 4993–5000

CERAMICS INTERNATIONAL

www.elsevier.com/locate/ceramint

Investigation of structural, magnetic and Mössbauer properties of Co^{2+} and Cu^{2+} substituted Ni–Zn nanoferrites

Sarveena[a,*], Gagan Kumar[b], Arun Kumar[a], R.K. Kotnala[c], Khalid M. Batoo[d], M. Singh[a]

[a]Department of Physics, Himachal Pradesh University, Shimla, India
[b]Department of Physics, IEC University, Atal Nagar, Kallujhanda, Baddi, India
[c]CSIR-National Physical Laboratory, Dr. K. S. Krishnan Road, Pusa, New Delhi, India
[d]King Abdullah Institute for Nanotechnology, King Saud University Riyadh, Saudi Arabia

Received 12 October 2015; received in revised form 26 November 2015; accepted 3 December 2015
Available online 10 December 2015

Abstract

We investigated the effects of Co^{2+} and Cu^{2+} substitution on the super-exchange interactions in Ni–Zn nanoferrites. The cation distribution technique was taken into account to explain the results. To authenticate the cation distribution, we have estimated the cation distribution in the light of X-ray diffraction method, Mössbauer spectroscopic analysis, and magnetization study. Statistical model based on the cation distribution was used to calculate the Curie temperature. The values of magneton number n_B and Curie temperature T_C calculated by using the cation distribution is found to be in agreement with the experimentally obtained values.

Keywords: Nanoferrites; Sol–gel auto combustion; Cation distribution; Mössbauer spectroscopy

1. Introduction

In recent years, the scientific literature has been replete with reports of magnetic nanoparticle synthesis, properties and novel applications [1]. In case of magnetic nanoparticles, the disruption in crystal structure at the surface can greatly influence the magnetic properties. The truncation of the lattice at the surface weakens exchange interactions and in many cases reduce coupling with neighboring particles. In particular, for spinel ferrites the magnetic exchange is dependent on the bond angles and lengths that are affected by the surface truncation. The bond bending commonly experienced on surfaces can produce profound changes in the magnetic properties of nanoparticles [2]. With the boom in the synthesis and characterization techniques in nanometer range, the research activities in the field of ferrites got a surge playing pivotal role in understanding the fundamentals of nanomagnetism [3].

Among the soft ferrites, Ni–Zn ferrites are one of the most versatile well-known mixed spinel ferrite, widely used because of its multipurpose and outstanding properties such as high resistivity, high dielectric, high initial permeability, mechanical hardness, high Curie temperature, chemical stability, high saturation magnetization and lower power loss [4]. Since cobalt is anisotropic in nature [5] and substitution of copper ions is known to improve the magnetic properties [6] therefore, interest in the present work was to see the effect of simultaneous substitution of cobalt and copper ions on the magnetic properties of Ni–Zn nanoferrites.

In order to obtain the cation distribution in the crystal lattice many researchers have applied different methods viz. X-ray diffraction [7] neutron diffraction [8] Mössbauer [9] and magnetization technique [10]. Although, the cation distribution of various ferrites has been studied extensively [7–10], the available literature on the verification of the cation distribution by different techniques is very scarce. Therefore, in the present

*Corresponding author.
E-mail address: sarveenahpu@gmail.com (Sarveena).

http://dx.doi.org/10.1016/j.ceramint.2015.12.012
0272-8842/

work, an attempt has been made to investigate the cation distribution from X-ray diffraction technique, Mössbauer spectroscopy analysis and magnetization method. The experimental results are then correlated to the cation distribution.

2. Experimental

The substituted Ni–Zn nanoferrites of composition $Ni_{0.58}Zn_{0.42}Co_xCu_yFe_{2-x-y}O_4$ ($x,y=0.0$, $x=0.1$, $y=0.05$, $x=0.2$, $y=0.05$) were prepared by sol–gel auto combustion method [11]. Stoichiometric amounts of A.R. grade Nickel Nitrate [$Ni(NO_3)_2.6H_2O$], Zinc Nitrate [$Zn(NO_3)_2.6H_2O$], Copper Nitrate [$Cu(NO_3)_2.3H_2O$], Cobalt Nitrate [$Co(NO_3).6H_2O$], Iron Nitrate [$Fe(NO_3)_3.9H_2O$], Citric Acid [$C_6H_8O_7.H_2O$] were used as starting raw materials. The stoichiometric mixture of above materials was dissolved in de-ionized water and small amount of ethylene glycol was added to it. As a kind of surfactant, it can effectively prevent the colloidal particle of chelate from being joined with each other. Hence to avoid this problem of agglomeration ethylene glycol was added. Citric acid has a double function, being the metal ion's complexant as well as fuel. In order for a high combustion rate, a molar ratio of the metal nitrates/citric acid of 1:1 was used. A small amount of ammonia solution was then added to adjust the pH value of clear solution at 7. The viscous sol attained by vaporizing solution at 80 °C. The sol was annealed at 200 °C to remove adsorbed water. During this process the gel self ignites and allow this to continue until the whole gel was burnt out to form a fluffy loose powder. The final powdered product was calcined at 500 °C for 5 h. The single phase was checked by X-ray diffraction studies, which were made by Cu-Kα radiation of wavelength 1.54 Å using Rigaku X-ray diffractometer. All XRD patterns were analyzed by using software of General Structure Analysis System (GSAS). Micro-structural features at high magnifications and selected area electron diffraction patterns were recorded using a transmission electron microscope of JEOL, USA. The measurement of magnetization as a function of applied field, and temperature was studied by using the Lake Shore's vibrating sample magnetometer. The room-temperature Mössbauer analysis was carried out by FAST Com Tec 07 09 06 and the spectra were analyzed by MossWinn 4.0.

3. Results and discussions

3.1. Structural study

The X-ray diffraction patterns with Rietveld refinement fitting of all the prepared samples are shown in Fig. 1. All XRD patterns were analyzed by using General Structure Analysis System software (GSAS). The XRD refinement for all the samples was continued until the convergence was reached $\chi^2 \sim 1$. The peak position and relative intensity of all diffraction peaks are observed to be matching well with the standard powder diffraction file of JCPDS Card no. 08-0234 thereby confirming the cubic spinel phase of the Fd3m space group without any signature of undesirable secondary phase. The particle size of the samples was calculated from the broadening of the Lorentzian peak (311) by using the Debye–Scherrer formula [12] and was observed to decrease (20–18 nm) with an estimated error of ± 0.2 while lattice parameter was observed to increase (8.348–8.406 Å). The estimated error in lattice parameter was observed to be ± 0.004. Since the ionic radius of Co^{2+} (0.745 Å), and Cu^{2+} (0.70 Å) ions is bigger as compared to Fe^{3+} ions (0.67 Å) therefore, the lattice expanded, and hence, the lattice constant increased. The theoretical lattice parameter (a_{th}) is calculated by using following relation [13]:

$$a_{th} = \frac{8}{3\sqrt{3}}\left[(r_A + R_o) + \sqrt{3}(r_B + R_o)\right] \quad (1)$$

where R_o is the radius of oxygen ions (1.32 Å). Fig. 2 shows the variation of theoretical lattice parameter (a_{th}) as a function of Co^{2+} and copper content. The theoretical lattice parameter was found to be increasing with the increasing substitution of Co^{2+} and copper ions thereby observed to follow the same trend as followed by the experimentally determined lattice parameter.

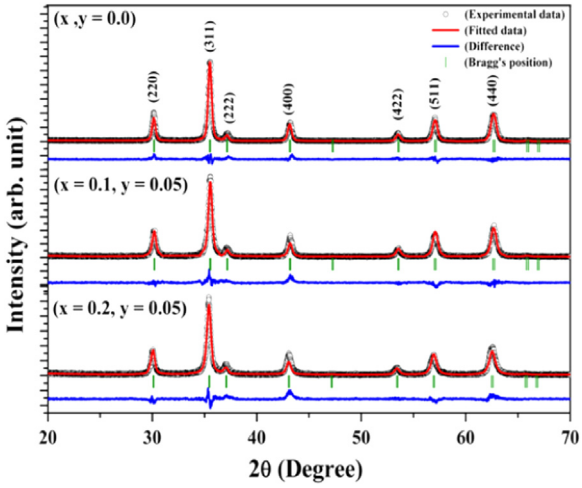

Fig. 1. Rietveld refined XRD pattern of $Ni_{0.58}Zn_{0.42}Co_xCu_yFe_{2-x-y}O_4$ nanoferrites.

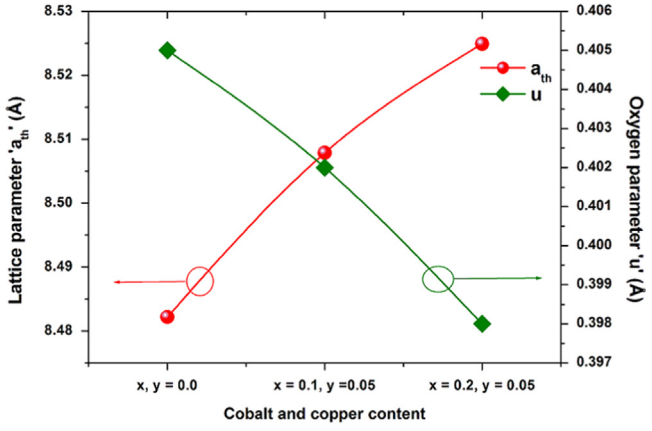

Fig. 2. Variation of theoretical lattice parameter and oxygen parameter for $Ni_{0.58}Zn_{0.42}Co_xCu_yFe_{2-x-y}O_4$ nanoferrites.

The O^{2-} ions in the spinel structure are generally not located at the exact positions of the FCC sublattice. Their detailed positions are determined by oxygen positional parameter u, which reflects adjustments of the structure to accommodate differences in the radius ratio of the cations in the A and B sites. Therefore, using values of a_{th}, R_o and r_A the oxygen positional parameter is calculated with the help of following expression [13]:

$$u = \left[\frac{1}{a_{th}\sqrt{3}}(r_A + R_o) + \frac{1}{4}\right] \quad (2)$$

The calculated values of 'u' are shown in Fig. 2. The observed trend in oxygen positional parameter shows that the anions at A-sites are moving towards the cations at tetrahedral (A) interstices. Since the overall strength of the magnetic interactions (A–B, A–A and B–B) depends on the bond lengths between the cations and cations–anion, therefore, in the present work we have made a theoretical attempt to calculate the same to get an information about the behavior of super-exchange interactions. The inter-ionic distances between the cations ($M_e - M_e$) (b, c, d, e, and f) and between the cation and anion ($M_e - O$) (p, q, r, and s) were calculated by using the relations reported by Gagan Kumar et al. [13]. The calculated values of inter-ionic distances between the cations (b, c, d, e, and f) and between the cation and anion (p, q, r and s) are given in Table 1. The distance between cation's was observed to be increasing with the increasing substitution of cobalt and copper ions. It was reported by Sagar E. Shirsath et al. [14] that increase in inter-ionic distances between cation–cation ($M_e - M_e$) results in weakening of the magnetic interactions thereby theoretical predictions suggests the weakening of magnetic interactions with the substitution of cobalt and copper ions.

The low resolution TEM, particle size distribution, SAED, and HRTEM images of powdered $Ni_{0.58}Zn_{0.42}Fe_2O_4$ ferrite nanoparticles are shown in Fig. 3(a–d). An overview of the TEM image of nanoparticles shows that the nanoparticles tend to agglomerate due to their mutual magnetic interaction. In the SAED image of synthesized particles, clearly visible distinct rings confirm good crystallinity of particles structure. The shape of the particles appears to be non-spherical. The average particle diameter was found to be ~16 nm which is in good agreement with XRD results. The observed crystallographic 'd' value of 2.100 Å correspond to lattice space of (400) plane of $Ni_{0.58}Zn_{0.42}Fe_2O_4$ nanoferrites. The crystallographic 'd' values are found to be in agreement with those obtained from XRD analysis.

Table 1
Inter-ionic distances between cation–anion (M_e–O) and cation–cation (M_e–M_e) for $Ni_{0.58}Zn_{0.42}Co_xCu_yFe_{2-x-y}O_4$ nanoferrites.

Parameter (Å)	x, y=0.0	x=0.1, y=0.05	x=0.2, y=0.05
b	2.964	2.969	2.972
c	3.476	3.482	3.486
d	3.630	3.636	3.640
e	5.445	5.455	5.460
f	5.133	5.142	5.147
p	1.83	1.86	1.90
q	2.27	2.23	2.17
r	4.34	4.28	4.15
s	3.78	3.77	3.76

3.2. Mössbauer study

Mössbauer spectroscopy is one of the important techniques which can measure the comparatively weak interactions between the nucleus and the surrounding electrons; as well as useful method for investigating the distribution of Fe ions over various sublattices. The room temperature ^{57}Fe Mössbauer spectra for synthesized nanoferrites are shown in Fig. 4. The dots represent experimental data points and the full curve is the least squares fit of the experimental spectrum. The best fits to the experimental data were obtained with two Zeeman sextets accounting for Fe^{3+} in the tetrahedral sites (A) and octahedral sites (B) of the spinel structure and third for quadrupole doublet (M). The fitted Mössbauer parameters are given in Table 2. The results showed some sort of relaxed ferromagnetic ordering. The appearance of a doublet indicates presence of some superparamagnetic contribution [15] imbedded in the long range ferromagnetic ordering which might be induced by fine particle size effects. The doublet can only be observed when the superparamagnetic relaxation of the nanoparticles occurs at a rate faster than the Mössbauer measurement time, given a time average zero magnetization. Due to the distribution of energy barriers, some nanoparticles relaxed faster and the other slower at a given temperature. Consequently, the sextet peak and doublet peak observed to appear simultaneously. From spectra, it is evident that the material is magnetically ordered. The values of quadrupole splitting for hyperfine spectra are observed to be negligibly small and are attributed to overall cubic symmetry. The isomer shifts relative to Fe metal are observed to be consistent with the high-spin Fe^{3+} state [16]. It is well known that the presence of Fe^{2+} deteroites the magnetic properties. Absence of Fe^{2+} confirmed from the isomer shift values clearly justified the quality of magnetic nanoparticles.

The internal magnetic field on nucleus can arise due to various interactions and can be written as:

$$H_{int} \approx H_{core} + H_{STHF} + H_{THF} + H_D \quad (3)$$

where H_{core} is the field due to polarization of the core s-electrons, H_{THF} and H_{STHF} are the transferred and super-transferred hyperfine fields respectively. The term, H_D is the dipolar field. Internal magnetic field will mainly depend upon the $H_{STHF,}$ which represents the super exchange interactions between two cations through oxygen anions, whereas H_{core}, H_{THF} and H_D will remain constant for all values of x and y. The hyperfine field was found to decrease with the increase in cobalt and copper substitution which corroborates well with the magnetization study. The decrease in internal field can be explained from the effect produced by substituted Co and Cu ions. The net magnetic field is mostly due to dominant $Fe_A^{3+} - O - Fe_B^{3+}$ linkage, because A–B ions interactions. As the two sublattice should be treated as a coupled system, the decrease in average magnetization at either site weakens A–B

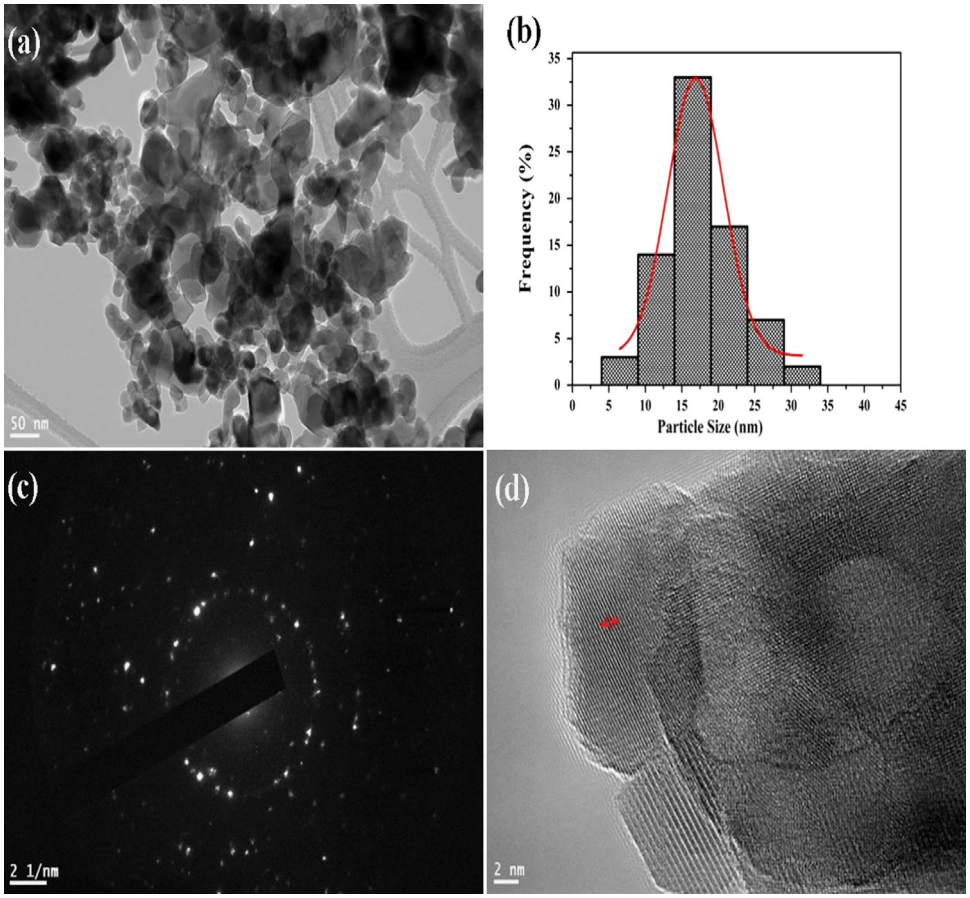

Fig. 3. (a) low resolution TEM, (b) particle size distribution, (c) SAED, and (d) HRTEM images of $Ni_{0.58}Zn_{0.42}Fe_2O_4$ nanoferrite.

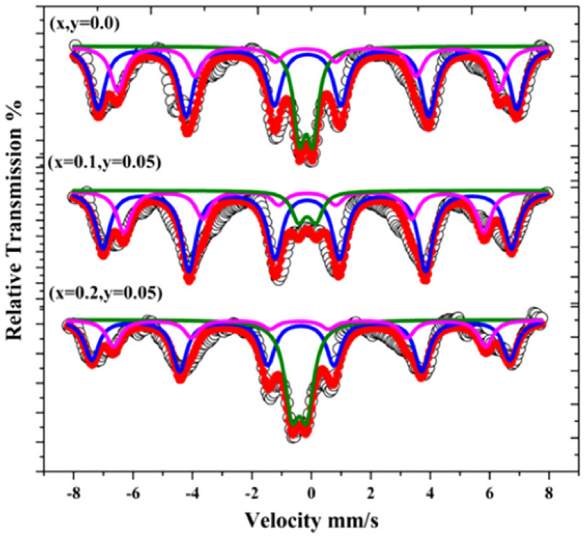

Fig. 4. Mössbauer spectra of $Ni_{0.58}Zn_{0.42}Co_xCu_yFe_{2-x-y}O_4$ nanoferrites.

interaction. In addition, *A–A* and *B–B* super transferred hyperfine interactions, which are strongly dependent on the angles between the spins, will tend to reduce the internal magnetic field. Thus weakening of $Fe_A^{3+}-O-Fe_B^{3+}$ super exchange interaction due to the substitution of Co and Cu ions reduced H_{STHF} thereby resulted in a net decrease of internal

Table 2
Mössbauer parameters for $Ni_{0.58}Zn_{0.42}Co_xCu_yFe_{2-x-y}O_4$ nanoferrites.

Sample	Site	WID	IS (mm/s)	QS (mm/s)	HMF (T)	Area (%)
$x, y=0$	*B*	0.51	−0.11	0.07	44.17	47.67
	A	0.37	−0.11	0.11	40.50	25.55
	M	0.58	−0.18	0.49	–	29.08
$x=0.1, y=0.05$	*B*	0.42	−0.12	0.04	43.34	53.68
	A	0.44	−0.13	0.06	39.59	33.25
	M	0.44	−0.19	0.58	–	13.07
$x=0.2, y=0.05$	*B*	0.55	−0.19	0.07	42.45	34.00
	A	0.51	−0.18	0.08	38.91	28.62
	M	0.58	−0.22	0.54	–	37.38

magnetic field at *A* as well as *B* site. Further, the variation can be correlated to the particle size on the basis of fluctuation of magnetization vectors in a direction close to an easy direction of magnetization. If the correlation time of the collective magnetization fluctuations is short relative to the observation time, the measured value of the magnetic field and consequently the hyperfine field will be reduced according to the equation [17]:

$$H_{hf}(V,T)=H_{hf}(V=\infty,T)\left[1-\frac{k_BT}{2KV}\right] \quad (4)$$

where k_B is the Boltzmann's constant, V is the particle volume and $V=\infty$, refers to a large crystals at temperature T in the

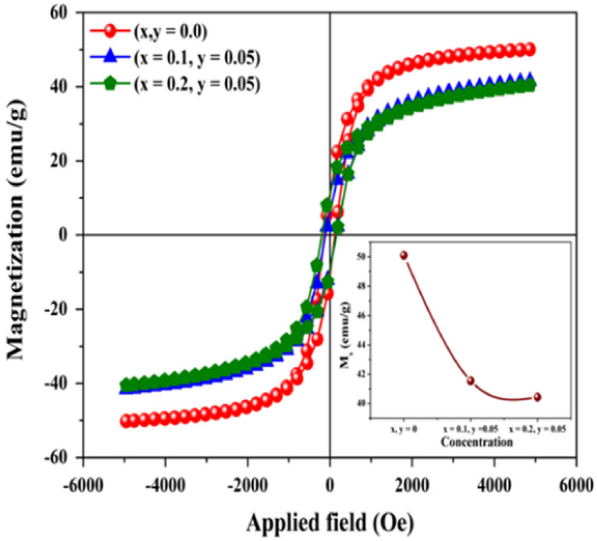

Fig. 5. Room temperature hysteresis curves of $Ni_{0.58}Zn_{0.42}Co_xCu_yFe_{2-x-y}O_4$ nanoferrites.

absence of collective magnetic excitations. Therefore, according to Eq. (4) the hyperfine filed deceases with the decrease in particle size since particles with different volumes will show different hyperfine splitting. In addition to increasing trend in inter-ionic distances between cation–cation, the decreasing behavior of magnetic hyperfine field is also indicating the weakening of super-exchange interaction.

3.3. Magnetic study

The room temperature *M–H* curves for synthesized nanoferrites are shown in Fig. 5. The saturation magnetization (shown in inset) was observed to be decreasing (50.15–40.39 emu/g) with the substitution of Co and Cu ions. It is known that in ferrites, the magnetic moment comes mainly from the parallel uncompensated electron spin of individual ion. The intensity of magnetization is, therefore, explained by considering the metal ion distribution and antiparallel spin alignment of the two sub-lattice sites as given by Neel's model [18]. According to Neel's model, there exists three kinds of interactions; the interactions between the various magnetic ions located at *A*-site (*A–A* interaction), the interaction between the various magnetic ions located at *B*-site (*B–B* interaction), and the interaction of magnetic ions at *A*-site with those at *B*-site (*A–B* interaction), of these *A–B* interaction predominates in strength over *A–A* and *B–B* interactions. *A–B* interaction aligns all magnetic spins at *A*-site in one direction and those at *B*-site in opposite direction thus constitute two saturated and magnetized sublattices at 0 K. Net magnetization of lattice is, therefore, the difference between magnetization of the *B*- and *A*-sublattices. As Co^{2+} and Cu^{2+} ions occupy *B*-sites and replace Fe^{3+} ions due to which magnetization of *B*-sublattice is decreased while the magnetization of *A*-sublattice is increased [19]. The observed behavior of magnetization indicated the weakening of *A–B* interactions. In order to confirm the variations in *A–B* super-exchange interactions, we have investigated the variations in magnetization as a function of temperature, in the range 373–773 K by applying a constant field of 1000 Oe, and the same are shown in Fig. 6(a). The *M–T* plots were used to determine the Curie temperature. The obtained values of Curie temperature are shown in Fig. 6(b). A decrease in Curie temperature was observed with the increase in Co^{2+} ions. Since Curie temperature is determined by an overall strength of the *A–B* exchange interactions, therefore, the substitution of copper and cobalt ions is resulting in the weakening of $Fe^{3+}(A)$–O^{2-}–$Fe^{3+}(B)$ super-exchange interactions due to which the Curie temperature is observed to decreasing and hence justifying the decreasing trend in saturation magnetization. In addition to decreasing trend in magnetic hyperfine interaction, the *M–H* behavior, and *M–T* results also confirmed the weakening of *A–B* interactions with the increasing substitution of Co^{2+} ions in the Ni–Zn nanoferrite matrix. In order to explain the observed behavior of exchange interaction we have made the cation distribution by using the Mössbauer spectroscopic analysis, magnetization technique and X-ray diffraction method.

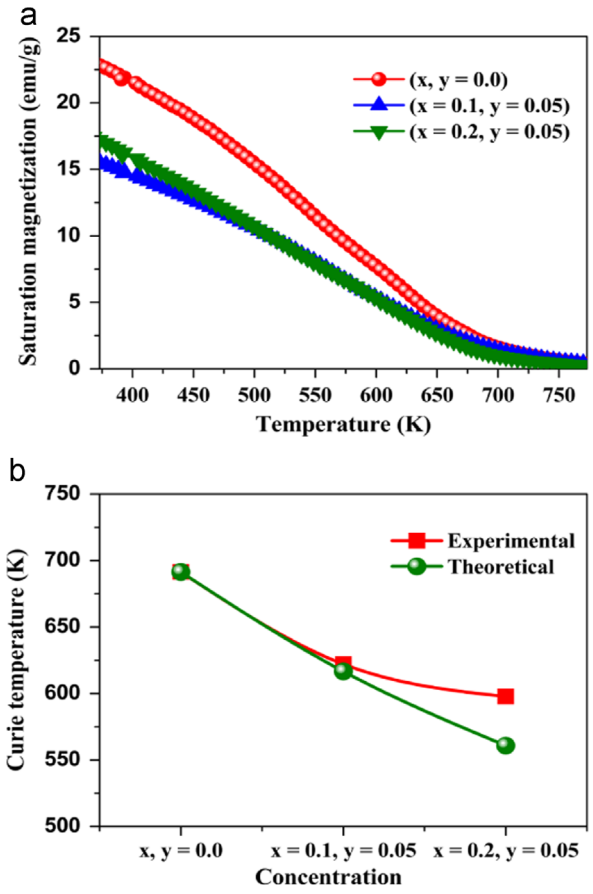

Fig. 6. (a)*M–T* curves, and (b) experimental and calculated values of Curie temperature for $Ni_{0.58}Zn_{0.42}Co_xCu_yFe_{2-x-y}O_4$ nanoferrites.

3.4. Cation distribution using X-ray diffraction technique

To estimate the distribution of cations among *A*- and *B*-sites, we have used the method as reported by S. S. More et al. [20]. In our study, we have taken the reflections (220), (400) and (440) to calculate the intensity ratio because the intensity ratios of planes I_{220}/I_{400}, I_{400}/I_{440} and I_{220}/I_{440} are considered

to be sensitive for the cation distribution. The temperature and absorption factors were not taken into account, because these factors do not affect the relative intensity calculation at room temperature [21]. To determine the cation distribution and its variation with composition, it is necessary to calculate for each composition the intensity ratios I_{220}/I_{400}, I_{400}/I_{440} and I_{220}/I_{440} expected for given arrangements of the cations and then compare them with the experimental values. The X-ray intensity for different planes (I_{hkl}) for powder specimen is calculated by using the following formula [21]:

$$I_{hkl} = |F_{hkl}|^2 . P . L_p \tag{5}$$

where F is structure factor, P is the multiplicity factor and Lp is the Lorentz polarization factor. The Lorentz polarization factor was calculated by using the following relation [21]:

$$L_p = \left(\frac{1+\cos^2 2\theta}{\sin^2\theta\cos\theta}\right) \tag{6}$$

The structure factors for different planes such as (220), (311), (400) and (440) were calculated by using the formulae reported by Furuhashi et al. [22] The multiplicity and ionic scattering factors were taken from the literature of Cullity [23]. The calculations were done by using various possible combinations of cations. The intensities for different planes were calculated for all the combinations and were then compared with those of experimental intensities. The estimated cation distribution for $Ni_{0.58}Zn_{0.42}Co_xCu_yFe_{2-x-y}O_4$ nano-ferrites at tetrahedral (A) and octahedral (B) sites along with the observed and calculated values for different intensity ratios is given in Table 3. The observed and calculated intensity ratios were found to be consistent with each other. It is evident that zinc ions preferred tetrahedral (A) site while Cu^{2+}, Co^{2+}, Ni^{2+} and Fe^{3+} ions preferred octahedral (B) site. Further, it was observed that when cobalt and copper ions were substituted in the Ni–Zn nanoferrite matrix, few zinc ions get migrated from A-site to B-site and therefore reduced the magnetization of B-sublattice.

3.5. Cation distribution using Mössbauer analysis and inversion parameter

The ratio of the areas under resonance curve of subspectra deduced from the measurements and the recoil free fraction of Fe at the octahedral and tetrahedral sites used to estimate the Fe occupancy for each site. We have calculated cation distribution of the different compositions and its inversion parameter by using the following relation:

$$\frac{n_A}{n_B} = \frac{z}{2-x-y-z} \tag{7}$$

where, n_A and n_B are the Fe ions at A- and B- site, respectively, x is cobalt content, y is copper content, and z is inversion parameter. The values of inversion parameter and cation distribution are summarized in Table 4 and are observed to be matching well with the cation distribution obtained from X-ray diffraction technique. Again the obtained cation distribution from Mössbauer analysis indicated that, when cobalt and copper ions were substituted in the Ni–Zn nanoferrite matrix, few zinc ions get migrated from A-site to B-site thereby, weakening the exchange interactions.

3.6. Cation distribution using magnetization technique

The cation distribution in the present system is derived from site preference energies and the magnetization method. According to the Neel's two sub-lattice model of ferrimagnetisms the magnetic moment per formula unit in Bohr magneton (μ_B); n_B^N is expressed as follow [24]:

$$n_B^N = M_B(X) - M_A(X) \tag{8}$$

where $M_B(X)$ and $M_A(X)$ are octahedral (B) and tetrahedral (A) sub lattice magnetic moments in Bohr magneton respectively. The values of magneton number n_B^N (saturation magnetization per formula unit in Bohr magneton) at room temperature were calculated, by using the following relation [24]:

$$n_B^N = \frac{\text{Sat.Magnetization} \times \text{Mol.weight}}{5585} \tag{9}$$

The $n_B^N(\mu_B)$ values were calculated by using the free ion magnetic moments of individual ions. The calculations have been done by using various possible combinations of cations. Table 5 represents the observed values of magnetic moments and the values calculated from the estimated cation distribution. It is evident by Table 5 that the observed and calculated values agree reasonably well with each other suggesting that the cation distribution obtained by using the magnetization method is principally acceptable.

Further, the Curie temperature was also evaluated theoretically by using the following statistical model based on the

Table 3
Cation distribution for $Ni_{0.58}Zn_{0.42}Co_xCu_yFe_{2-x-y}O_4$ nanoferrites obtained from X-ray diffraction method.

Sample	Cation distribution	I_{220}/I_{400}		I_{400}/I_{440}		I_{220}/I_{440}	
		Obs.	Cal.	Obs.	Cal.	Obs.	Cal.
x, y=0.0	$(Zn_{0.42}Fe_{0.95})_A$ $[Ni_{0.58}Fe_{1.05}]_B$	1.50	1.53	0.72	0.44	1.08	0.68
x=0.1, y=0.05	$(Zn_{0.35}Ni_{0.05}Co_{0.01}Fe_{0.87})_A$ $[Zn_{0.07}Ni_{0.53}Cu_{0.05}Co_{0.09}Fe_{0.98}]_B$	1.20	1.28	0.69	0.48	0.83	0.62
x=0.2, y=0.05	$(Zn_{0.34}Ni_{0.1}Cu_{0.01}Co_{0.02}Fe_{0.82})_A$ $[Zn_{0.08}Ni_{0.48}Cu_{0.04}Co_{0.18}Fe_{0.93}]_B$	1.18	1.03	0.71	0.53	0.84	0.54

Table 4
Cation distribution for $Ni_{0.58}Zn_{0.42}Co_xCu_yFe_{2-x-y}O_4$ nanoferrites obtained from Mössbauer analysis and inversion parameter.

Sample	Cation distribution	Inversion parameter (z)
x, y=0.0	$(Zn_{0.42}Fe_{0.95})_A$ $[Ni_{0.58}Fe_{1.05}]_B$	0.95
x=0.1, y=0.05	$(Zn_{0.35}Ni_{0.05}Cu_{0.01}Co_{0.01}Fe_{0.87})_A$ $[Zn_{0.07}Ni_{0.53}Cu_{0.04}Co_{0.09}Fe_{0.98}]_B$	0.87
x=0.2, y=0.05	$(Zn_{0.34}Ni_{0.1}Cu_{0.01}Co_{0.03}Fe_{0.82})_A$ $[Zn_{0.08}Ni_{0.48}Cu_{0.04}Co_{0.17}Fe_{0.93}]_B$	0.82

Table 5
Cation distribution for $Ni_{0.58}Zn_{0.42}Co_xCu_yFe_{2-x-y}O_4$ nanoferrites obtained from magnetization technique.

Sample	Cation distribution	n_B (μ_B)	
		Obs.	Cal.
x, y=0.0	$(Zn_{0.42}Fe_{0.91})_A$ $[Ni_{0.58}Fe_{1.09}]_B$	2.13	2.06
x=0.1, y=0.05	$(Zn_{0.35}Ni_{0.06}Cu_{0.01}Co_{0.01}Fe_{0.87})_A$ $[Zn_{0.07}Ni_{0.52}Cu_{0.04}Co_{0.09}Fe_{0.98}]_B$	1.77	1.76
x=0.2, y=0.05	$(Zn_{0.34}Ni_{0.11}Cu_{0.01}Co_{0.03}Fe_{0.82})_A$ $[Zn_{0.08}Ni_{0.47}Cu_{0.04}Co_{0.17}Fe_{0.93}]_B$	1.73	1.74

cation distribution [25]:

$$T_C(x) = \left[\frac{M(x=0)T_C(x=0)n(x)}{n(x=0)M(x)}\right] \quad (10)$$

Here, $M(x)$ is the relative weighted total magnetic ions per formula unit, calculated by considering the weighting of the magnetic ion concentration for the substituted ferrite to that of the unsubstituted one while $n(x)$ is the number of interactions per magnetic ion per formula unit, expressed as follow

$$n(x) = \sum_{i,j=1}^{2} A_i B_j \mu_i \mu_j \quad (11)$$

where A_i and B_j are the fraction of magnetic ions on the A- and B-sites, respectively, while μ_i and μ_j are the magnetic moments of the cation involved. Theoretical estimated Curie temperature values are shown in Fig. 6(b) and are in good agreement with the values obtained from M–T results and thus supporting the validity of cation distribution.

4. Conclusions

We have made an attempt to estimate the cation distribution by X-ray diffraction method, magnetization technique and Mössbauer spectroscopic analysis, and the same was observed to be consistent with each other. The theoretical interpretations based on the cation distribution followed by experimental evidences, M–H, M–T, and Mössbauer spectroscopy, revealed the weakening of A–B super-exchange interactions with the incorporation of Co^{2+} and Cu^{2+} content in the Ni–Zn nanoferrite matrix.

Acknowledgments

One of the authors (Sarveena) is thankful to I.U.A.C, New Delhi, India, for financial support through UFUP project under grant no. UFR 51308. The author K. M. Batoo would like to extend his sincere appreciation to the Deanship of Scientific Research at King Saud University for its funding through the Research Group Project no. RGP VPP-290

References

[1] B.L. Cushing, V.L. Kolesnichenko, C.J. O'Connor, Recent advances in the liquid-phase syntheses of inorganic nanoparticles, J. Chem. Rev. 104 (2004) 3893–3946.
[2] J.L. Dormann, D. Fiorani, E. Tronc, Magnetic relaxation in fine-particle systems, Adv. Chem. Phys. 98 (1997) 283–494.
[3] C. Zhou, T.C. Schulthess, D.P. Landau, Monte Carlo simulations of $NiFe_2O_4$ nanoparticles, J. Appl. Phys. 99 (2006) 08H906.
[4] I. Ismail, M. Hashim, K.A. Matori, R. Alias, J.J. Hassan, Milling time and BPR dependence on permeability and losses of $Ni_{0.5}Zn_{0.5}Fe_2O_4$ synthesized via mechanical alloying, J. Magn. Magn. Mater. 323 (2011) 1470–1476.
[5] Gagan Kumar, J. Chand, A. Dogra, R.K. Kotnala, M. Singh, Improvement in electrical and magnetic properties of mixed Mg–Al–Mn ferrite system synthesized by citrate precursor technique, J. Phys. Chem. Solids 71 (2010) 375–380.
[6] M.F. Huq, D.K. Saha, R. Ahmed, Z.H. Mahmood, Ni–Cu–Zn ferrite research: a brief review, J. Sci. Res. 5 (2013) 215–234.
[7] S.S. Jadhav, Sagar E. Shirsath, S.M. Patange, K.M. Jadhav, Effect of Zn substitution on magnetic properties of nanocrystalline cobalt ferrite, J. Appl. Phys. 108 (2010) 093920.
[8] A.K. Ghatage, S.A. Patil, S.K. Paranjpe, Neutron diffraction study of chromium substituted nickel ferrite, Solid State Commun. 98 (1996) 885–888.
[9] R.K. Sharma, V. Sebastian, N. Lakshmi, K. Venugopalan, V.R. Reddy, A. Gupta, Variation of structural and hyperfine parameters in nanoparticles of Cr-substituted Co–Zn ferrites, Phys. Rev. B. 75 (2007) 144419.
[10] A.M. Wahba, M.B. Mohamed, Structural and magnetic characterization and cation distribution of nanocrystalline $Co_xFe_{3-x}O_4$ ferrites, J. Magn. Magn. Mater. 378 (2015) 246–252.
[11] A. Sutka, G. Mezinskis, Sol–gel auto-combustion synthesis of spinel-type ferrite nanomaterials, Front. Mater. Sci. 6 (2012) 128–141.
[12] Virender Pratap Singh, Gagan Kumar, Jyoti Shah, Arun Kumar, M. Dhiman, R.K. Kotnala, M. Singh, Investigation of super-exchange interactions in $BaHo_xFe_{12-x}O_{19}$ $(0.1 \le x \le 0.4)$ nanohexaferrites and exploration at ultra high frequency region, Ceram. Int. 41 (2015) 11693–11701.
[13] Gagan Kumar, Jyoti Shah, R.K. Kotnala, Virender Pratap Singh, Sarveena, Godawari Garg, Sagar E. Shirsath, Khalid M. Batoo, M. Singh, Superparamagnetic behaviour and evidence of weakening in super-exchange interactions with the substitution of Gd^{3+} ions in the Mg–Mn nanoferrite matrix, Mater. Res. Bull. 63 (2015) 216–225.
[14] Sagar E. Shirsath, R.H. Kadam, S.M. Patange, M.L. Mane, A. Ghasemi, A. Morisako, Enhanced magnetic properties of Dy^{3+} substituted Ni–Cu–Zn ferrite nanoparticles, Appl. Phys. Lett. 100 (2012) 042407.
[15] S. Thakur, S.C. Katyal, A. Gupta, V.R. Reddy, M. Singh, Room temperature ferromagnetic ordering in indium substituted nano-nickel-zinc ferrite, J. Appl. Phys. 105 (2009) 07A521.
[16] D.P.E. Dickson, F.J. Berry, Mössbauer Spectroscopy, Cambridge University Press, London, 1986.
[17] J. Gagan Kumar, R.K. Shah, V.P. Kotnala, M. Singh, S.E. Dhiman, M. Shirsath, K.M. Shahbuddin, Batoo, M. Singh, Mössbauer spectroscopic analysis and temperature dependent electrical study of $Mg_{0.9}Mn_{0.1}Gd_yFe_{2-y}O_4$ nanoferrites, J. Magn. Magn. Mater. 390 (2015) 50–55.

[18] L. Neel, Propriétés magnétiques des ferrites: ferrimagnétisme et antiferromagnétisme, Ann. Phys. 3 (1948) 98–137.
[19] C.F. Zhang, X.C. Zhong, H.Y. Yu, Z.W. Liu, D.C. Zeng, Effects of cobalt doping on the microstructure and magnetic properties of Mn–Zn ferrites prepared by the co-precipitation method, Physica B 404 (2009) 2327–2331.
[20] S.S. More, R.H. Kadam, A.B. Kadam, A.R. Shite, D.R. Mane, K. M. Jadhav, Cation distribution in nanocrystalline Al^{3+} and Cr^{3+} co-substituted $CoFe_2O_4$, J. Alloy. Compd. 502 (2010) 477–479.
[21] P. Porta, F.S. Stone, R.G. Turner, The distribution of nickel ions among octahedral and tetrahedral sites in $NiAl_2O_4$–$MgAl_2O_4$ solid solutions, J. Solid State Chem. 11 (1974) 135–147.
[22] H. Furuhashi, M. Inagaki, S. Naka, Determination of cation distribution in spinels by X-ray diffraction method, J. Inorg. Nucl. Chem. 35 (1973) 3009–3014.
[23] B.D. Cullity, Elements of X-ray Diffraction, Addison Wesley, USA, 1956, p. 474.
[24] J. Smit, Magnetic Properties of Materials, Intra-University Electronics Series, 1971.
[25] S.M. Patange, Sagar E. Shirsath, G.S. Jangam, K.S. Lohar, S.S. Jadhav, K.M. Jadhav, Rietveld structure refinement, cation distribution and magnetic properties of Al substituted $NiFe_2O_4$ nanoparticles, J. Appl. Phys. 109 (2011) 053909.